Journal of Marine Systems 243 (2024) 103952

Contents lists available at ScienceDirect

Journal of Marine Systems

journal homepage: www.elsevier.com/locate/jmarsys

Clustering as a mechanism for enhanced reaction of buoyant species

Jamie Meacham [a,*], Pavel Berloff [a,b]

[a] Department of Mathematics, Imperial College London, Huxley Building, 180 Queen's Gate, London, SW7 2AZ, UK
[b] Institute of Numerical Mathematics, Russian Academy of Sciences, Gubkina 8, Moscow, 119333, Russia

ARTICLE INFO

Keywords:
Clustering
Lagrangian
Turbulent mixing
Oceanic processes

ABSTRACT

Buoyant material has a tendency to form dense clusters at the ocean surface. This has been observed in distributions of marine life and floating plastic contaminants. The main mechanism behind this is that particles with positive/neutral buoyancy do not behave as passive tracers in stratified flows. It could be expected that coextensive clustering between plankton and toxic ocean contaminants could lead to enhanced ecological risk. However, such interactions cannot be sufficiently modelled in a standard passive tracer approximation. Given the large uncertainty in the form of converging currents and how to model interactions of buoyant tracers, we opt for an idealised modelling approach. The simplicity of our model allows easy interpretation of the novel physical considerations. We demonstrate that the global dynamics of our biogeochemical model are significantly altered by clustering forces. Most notably, a new balance in the ecosystem exists in which reactions are dominated entirely by those within the dense clusters. This greatly enhances the impact of destructive pollutants through efficient mixing. There is evidence that this equilibrium will be robust moving to more complex and realistic models.

1. Introduction

The tendency of buoyant material at the ocean surface to form clusters is well documented in both observations (Gower et al., 2006) and from a theoretical perspective (Klyatskin, 2003; Koshel et al., 2019; Stepanov et al., 2020a,b). Interest in this phenomenon has increased primarily due to the observation of dense aggregations of floating plastic pollution, forming the so called 'Garbage patches'. It could be expected that the high concentration of harmful pollutants in these patches leads to increased ecological risk to ocean-borne populations. However, uncertainty exists as to the extent of this risk, due to a lack of modelling of the issue and uncertainty in measurements of the global plastic distribution (van Sebille et al., 2015).

Biogeochemical tracers, such as plankton populations, are treated as purely passive in most standard methodologies. Passive tracers are advected by the fully three-dimensional, incompressible velocity field of the ocean currents. Such methods have been immensely successful in the past, showing significant predictive skill (Flynn and McGillicuddy, 2018). However, these particles can never form clusters through the action of the currents alone, due to the conservation of density along Lagrangian paths.

In reality, plankton populations are not passive. They demonstrate a range of buoyancies in water that can depend on the time of year and the general environment, as well as the individual species. Some plankton species are known to have methods to regulate their buoyancy, in part to retain their depth and also to maximise exposure to sunlight and nutrient sources. The dense streaks of plankton observed in satellite chlorophyll measurements are also qualitatively reminiscent of clusters observed in numerical experiments.

Heterogeneity in the spatial distribution of plankton populations, often referred to as "patchiness", is generated through a number of mechanisms (Matthews and Brindley, 1997). Diffusivity instability is a primary mechanism that is generally considered, and is a consequence of the differing transport properties of marine species. However, this process is known to act at small scales, typically the kilometre scale and below (Della Rossa et al., 2013). Meanwhile, observations of chlorophyll distributions show heterogeneity at all scales, particularly at the submesoscale/mesoscale boundary (~10–50 km), which is the focus of our study. At this scale, coupling of the plankton distribution to flow structures is self-evident (Martin, 2003). Examples include the high concentrations often found at the core or boundary of geostrophic vortices. Chaotic stirring by the geostrophic flow alone could cause this coupling, but only through the reorganisation of existing concentration gradients. Diffusivity instability is even less likely to be a source of these larger scale gradients, since the horizontal ocean currents typically cascade enstrophy of a tracer distribution towards smaller scales as opposed to larger scales. Mixing by ocean currents is also

* Corresponding author.
E-mail address: jom20@ic.ac.uk (J. Meacham).

https://doi.org/10.1016/j.jmarsys.2023.103952
Received 14 March 2023; Received in revised form 17 November 2023; Accepted 30 November 2023
Available online 1 December 2023

incapable of producing concentration gradients of passive tracer, due to incompressibility. By considering how positive buoyancy of plankton leads to deviations from passive flow, we arrive at a purely geophysical mechanism that can produce sufficient heterogeneity at larger scales.

Even neutrally buoyant particles behave in a fundamentally different way to passive tracers, as has been shown by modelling fully inertial particles in three-dimensional stratified flows (Reartes and Mininni, 2023). Most notably, they have a tendency to form a layer around the vertical level of their neutral buoyancy. This provides a mechanism for cluster formation, since if the vertical flow of particles is inhibited by buoyancy forces, then floating material will predominantly follow the horizontal flow. Even in an incompressible flow, the horizontal component can be convergent, leading to clusterising and an increase of concentration along Lagrangian paths.

Motivated by the observations from three-dimensional studies, a simple model of floating tracers has been developed. If we consider an idealised, incompressible ocean bounded by a rigid lid, we can model buoyant tracers as being trapped in a very thin layer just below the surface. The problem then reduces to a quasi two-dimensional model, where particles are advected by the surface currents alone. This model has been used previously to investigate cluster formation of inert floating tracers (Koshel et al., 2019; Stepanov et al., 2020a,b; Meacham and Berloff, 2023) and to determine the location of accumulation zones of floating microplastic (Onink et al., 2019). For the first time, we extend the model to reacting tracers. Most importantly, we allow for interactions between buoyant and passive tracers, and find that there are implications for the form of reaction coefficients. This allows us to construct a simplified model of the interactions between passive nutrients, neutrally buoyant plankton and floating contaminants (such as microplastics).

Many classical NPZ (nutrient, phytoplankton, zooplankton) models contain complex interaction terms, which allow for chaotic dynamics. These lead to novel behaviours, mimicking the rich dynamics of the marine ecosystem, such as seasonal blooms (Franks, 2002). Even more complex operational/predictive models will contain a large number of species and represent a myriad of reactions between them. This realism enhances the reproduction of observed distributions, but comes at the cost of interpretability.

For clustering problems, the large uncertainty in the form of convergent surface currents, as well as the lack of previous modelling motivates a 'ground up' approach, beginning with idealised simulations. We found that considering floating tracers introduces a host of new physical considerations. Determining the correct form of these reacting models was not trivial, and utilising a simple model helps in this endeavour. The insights gained in our framework are not unique to idealised models and can be readily extended to more complex systems, which promises a fruitful line of future research.

We show two important factors: clustering has a minimal impact on passive/floating tracer interactions but completely alters the dynamical character of the system for interactions between species of buoyant tracers. Coextensive clustering amplifies the strength of reactions, with severe implications for the destructive effect of contaminants on marine populations.

The model allows for an asymptotic equilibrium solution, which can be verified through numerical experiments. Surprisingly, this equilibrium is totally independent of the velocity field, which bodes well for the parameterisation of clustering in realistic ocean models.

Inclusion of a physical effect that is most familiar to Lagrangian modellers, buoyant clustering, leads to a strong and novel coupling between oceanographic fluid dynamics and biological population dynamics. This leads to a situation where accurate modelling will necessitate interdisciplinary communication. We hope our idealised investigation motivates this.

2. Methods

2.1. Idealised biogeochemical modelling

To model biogeochemical reactions, we begin with the most basic representation (Franks, 2002), that has been used previously in applications where simplicity is desired (Prend et al., 2021). This consists of a set of coupled ODEs, deliberately constructed to tend towards an analytic equilibrium. We can characterise the impact of clustering on this model by observing the change in the equilibrium state. At first, only nutrients and phytoplankton masses are involved. Subsequently, a third species is introduced to represent destructive contaminants such as toxic POPs (Persistent Organic Pollutants).

2.1.1. NP model

The first model is

$$\frac{dN}{dt} = -\mu NP - \lambda(N - N_D), \tag{1}$$

$$\frac{dP}{dt} = \mu NP - \lambda P, \tag{2}$$

where N is the total mass of nutrients and P is the total mass of plankton. It contains terms to model the consumption of nutrients by plankton, and also the natural decay of both species. To accommodate a steady state, we require a source of nutrients into the system to balance the decay, the rate of which is set by λN_D. In a more realistic model, this might be represented by the delayed reconstitution of dead plankton as nutrients, leading to a conservation of biomass. The idealised model approximates this behaviour. Integrating these equations will show that P evolves similarly to a logistic growth curve. The system tends to a final equilibrium with values $N_\infty = \frac{\lambda}{\mu}$, and $P_\infty = N_D - N_\infty$. Importantly, this system permits a quantity $Q = N - N_D + P$ which satisfies:

$$\frac{dQ}{dt} = -\lambda Q. \tag{3}$$

This 'conservation of biomass' is an essential component of the model, and justifies the form of the coefficients μ, λ, which allow for this conservation.

2.1.2. NPC model

To model the impact of pollutants, we need a system that can represent the interactions between pollutants and plankton. Motivated by the simple idealised form of Eqs. (1)–(2), we propose the inclusion of a contaminant mass C that obeys:

$$\frac{dC}{dt} = -\mu PC - \lambda(C - C_D), \tag{4}$$

with Eq. (2) also modified as follows:

$$\frac{dP}{dt} = \mu NP - \mu PC - \lambda P \tag{5}$$

This captures the continual input of contaminants to the ocean, similar to the feeding of nutrients into the system in Eq. (1). It also models the ecological effect of contaminant as mutual destruction of both species. Plankton consumes toxic contaminant and is eliminated in the process.

If we define $\tilde{N} = N - C$, we can see that this system is identical to Eqs. (1)–(2). The result is that the plankton mass will evolve in a similar fashion, but with reduced carrying capacity. This will no longer be the case once we introduce the clustering process. This is because there is a distinction between species which are purely passive (follow the full three dimensional ocean currents) and the floating material (which only follows the surface flow) that modifies the form of interactions between them.

This model also admits a 'conserved' quantity $Q = N - N_D + P - C + C_D$, satisfying Eq. (3). This still represents a conservation of biomass. However, destruction of plankton by the contaminant removes biomass from the system, leading to the reduced carrying capacity.

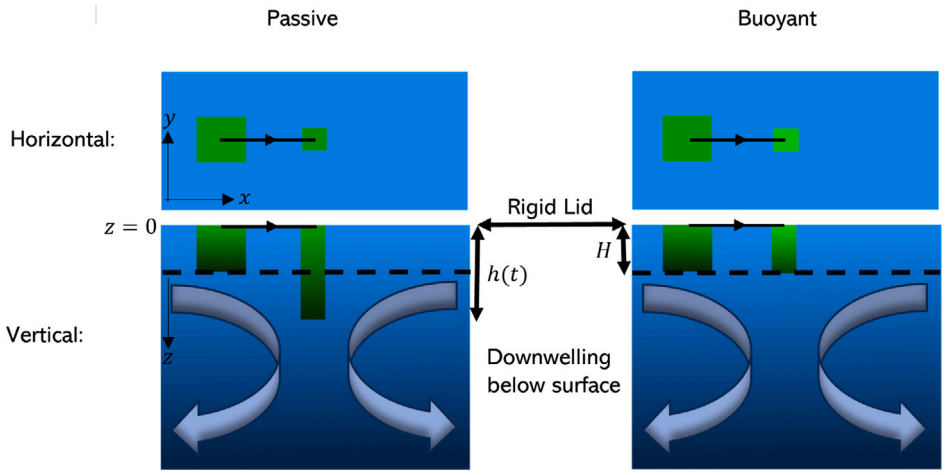

Fig. 1. Both passive and buoyant tracers can be modelled at the surface. Converging surface currents will cause the top area, A, of a material element to contract (see horizontal view). For the passive tracer, this will be matched by the corresponding downwelling just beneath the surface, which increases the depth of the column (see vertical view). The depth of the column, $h(t)$ can be directly solved for using Eq. (15) and will satisfy $hA = \text{constant}$. This ensures the mass of passive tracer within the element is conserved. Buoyant tracers are trapped in a thin layer below the surface with no vertical velocity, so the convergence leads to an increase in concentration. This also explains the form of the reaction coefficients in Eqs. (22)–(25).

The equilibrium state is found to be modified by the inclusion of contaminant as follows:

$$N = N_\infty \frac{N_D}{N_D - C_D}, \tag{6}$$

$$P = P_\infty - C_D, \tag{7}$$

$$C = N_\infty \left(\frac{N_D}{N_D - C_D} - 1 \right), \tag{8}$$

where N_∞ and P_∞ are the equilibrium values of the NP model as defined in the previous section.

2.2. Tracer models

Our idealised ocean is bounded by a rigid lid at the surface. Both passive and buoyant particles at this surface will follow Lagrangian paths restricted to the horizontal plane. This is because there is no vertical velocity at the rigid lid by definition. The equation we must solve for the surface Lagrangian paths is:

$$\frac{d}{dt}\mathbf{x}(t;\mathbf{x}_0) = \mathbf{u}(\mathbf{x}(t;\mathbf{x}_0), t)\,, \tag{9}$$

$$\mathbf{x}(0;\mathbf{x}_0) = \mathbf{x}_0 \tag{10}$$

where $\mathbf{u}$ is the two-dimensional surface flow, $\mathbf{x} = (x, y)$ are the horizontal surface coordinates $\mathbf{x}_0$ is the initial location of the Lagrangian path.

Consider a small patch of Lagrangian particles at the surface. It can be shown that the area, A, of that patch satisfies:

$$\frac{dA}{dt} = A\nabla \cdot \mathbf{u} \tag{11}$$

where $\frac{d}{dt}$ is the material derivative, following the Lagrangian paths (See Appendix A for details).

We can construct the dynamics for the concentration of buoyant tracers and the density of passive tracers at the surface. We do this by considering material volumes that are bounded above by the rigid lid and reach just below the ocean surface.

For buoyant tracers trapped in a thin layer of thickness H, the volume of a material element will be proportional to AH. The mass inside such an element should be conserved. This implies the concentration, C, of buoyant tracer will be related to the area by $C \sim 1/A$, since H is constant.

For passive tracers, the density of tracer should be conserved along the Lagrangian paths. If the mass of a material element is also conserved, it follows that the volume should be invariant. We can account for this by considering the vertical velocity of passive tracer just below the surface. In an incompressible ocean:

$$\nabla \cdot \mathbf{u}_{3D} = \frac{\partial u}{\partial x} + \frac{\partial v}{\partial y} + \frac{\partial w}{\partial z} = 0 \tag{12}$$

where $\mathbf{u}_{3D}$ is the fully three-dimensional flow in the ocean interior. By a Taylor expansion, we can find the vertical velocity just below the ocean surface:

$$w(x, y, z) \approx w(x, y, 0) + z\frac{\partial w}{\partial z}|_{z=0} \tag{13}$$

Using Eq. (12), and the rigid lid boundary condition ($w(x, y, z = 0) = 0$), we can rearrange this:

$$w(x, y, z) \approx -z\nabla \cdot \mathbf{u} \tag{14}$$

with the two dimensional surface divergence on the right hand side, identically to Eq. (11). Therefore, the depth of a material volume, h, of passive tracer at the surface satisfies:

$$\frac{dh}{dt} = -h\nabla \cdot \mathbf{u} \tag{15}$$

This is consistent with the conservation of volume of passive tracer, since combining Eqs. (11) and (15) implies that $Ah \sim constant$.

See Fig. 1 for an illustration of a material volume of both passive and buoyant tracers. Both volumes are attached to the surface. However, for the passive element, any contraction of the top surface area is matched by a stretching of the column depth to preserve volume. The fixed layer depth of the buoyant tracers means that surface convergences leads to an increase in concentration, as the volume of the element decreases proportionally to the area.

Combining these observations, the density of passive tracer, ρ, following a surface Lagrangian path is constant.

$$\frac{d\rho}{dt} = 0\,, \tag{16}$$

while the local depth of the column satisfies:

$$\frac{dh}{dt} = -h\nabla \cdot \mathbf{u}\,, \tag{17}$$

but the concentration of buoyant tracer satisfies:

$$\frac{dC}{dt} = -C\nabla \cdot \mathbf{u}\,, \tag{18}$$

while the local depth is constant. See Fig. 1 for an illustration of both material volumes and how they differ. We can combine this model of surface tracers with the biogeochemical model by introducing sources and sinks on the right hand sides.

2.2.1. Surface masses

Our Lagrangian models will produce local information through solving equations for concentration and density along Lagrangian paths. However, the real quantities we are interested in are global. For instance, what is the overall impact of clustering on the total plankton population?

In order to assess this, we need to integrate our density distributions to evaluate global masses.

For buoyant tracers, this is straightforwardly:

$$M_C = \int_D d^2\mathbf{x}\, C(\mathbf{x}, t)\,, \tag{19}$$

where D is the horizontal ocean surface.

For passive tracers we must consider the varying depth of the column, so the total mass is:

$$M_\rho = \int_D d^2\mathbf{x}\, h(\mathbf{x}, t)\rho(\mathbf{x}, t)\,, \tag{20}$$

$$\frac{\partial h}{\partial t} + \mathbf{u}\cdot\nabla h = -h\nabla\cdot\mathbf{u},$$

$$h(\mathbf{x}, 0) = 1.$$

We can show that these two quantities are constant in time for particles satisfying Eqs. (16) and (18), respectively. See Appendix A for details.

2.2.2. NP tracer model

We start by investigating a nutrient-plankton (NP) model, with two components. Defining the nutrient density n and the plankton concentration p, we integrate the positions of the Lagrangian paths at the horizontal surface:

$$\frac{d\mathbf{x}}{dt}(t; \mathbf{x}_0) = \mathbf{u}(\mathbf{x}, t)\,, \tag{21}$$

then, along each Lagrangian path, we integrate the nutrient density, plankton concentration and the factor by which the passive tracer column has stretched:

$$\frac{dn}{dt} = -\frac{\mu}{h}np - \lambda(n - n_D)\,, \tag{22}$$

$$\frac{dp}{dt} = -p\nabla\cdot\mathbf{u} + \mu np - \lambda p\,, \tag{23}$$

$$\frac{dh}{dt} = -h\nabla\cdot\mathbf{u}\,, \tag{24}$$

$$h(0) = 1\,. \tag{25}$$

To understand the factor of $1/h$ in the mutual reaction of nutrients and plankton in Eq. (22), consider Fig. 1. At an area of downwelling, the passive column gets deeper, whilst the buoyant tracer remains at a constant depth, this means that the mass of nutrients available to react with plankton is reduced, as the cross section between the two material volumes decreases. The proportion of the column of passive nutrients that overlaps with the buoyant plankton is exactly $1/h$, leading to a proportionate reduction in the reactivity.

As in the previous section, surface masses are:

$$P = \int_D d^2\mathbf{x}\, p(\mathbf{x}, t) \tag{26}$$

$$N = \int_D d^2\mathbf{x}\, h(\mathbf{x}, t)\, n(\mathbf{x}, t) \tag{27}$$

These surface masses obey Eq. (3) for $Q = N + P - N_D$. It can also be shown that the surface masses exactly satisfy Eqs. (1)–(2) and details of this are contained in Appendix A. Both factors depend on the form of the coefficients. For instance, we must have the same μ and λ in Eqs. (22) and (23) to conserve biomass (Franks, 2002). This is a desirable quality of our system, since it enhances the physical realism and allows for easier interpretability.

Once we make this imposition, it can be shown that the global masses exactly satisfy Eqs. (1)–(2). Hence, there is no impact of clustering in this model. This is to be expected, since there is no coextensive clustering of species, which will be required to increase reaction rates. Adding in a buoyant contaminant completely changes this.

2.2.3. NPC tracer model

The NP model above can be extended to include a buoyant contaminant, meant to represent a destructive toxic pollutant such as microplastic waste.

Again, we solve for the Lagrangian paths. We now also integrate the contaminant concentration, c, along each path:

$$\frac{dn}{dt} = -\frac{\mu}{h}np - \lambda(n - n_D)\,, \tag{28}$$

$$\frac{dp}{dt} = -p\nabla\cdot\mathbf{u} + \mu np - \mu pc - \lambda p\,, \tag{29}$$

$$\frac{dc}{dt} = -c\nabla\cdot\mathbf{u} - \mu pc - \lambda\left(c - \frac{c_D}{A}\right)\,, \tag{30}$$

$$\frac{dh}{dt} = -h\nabla\cdot\mathbf{u}\,, \tag{31}$$

$$h = 1/A\,, \tag{32}$$

$$h(0) = 1\,. \tag{33}$$

Here, the impact of contaminants is modelled as mutual destruction of both species. Plankton ingests pollutants and is destroyed in the process. Contaminants are continously input uniformly across the domain, represented by the term $-\lambda c_D/A$. The variable A is the scaling factor of the area of the top surface of the material volume. By scaling the contaminant source by $1/A$, we account for the fact that the volume of the material volume of a buoyant tracer can change over time (see Fig. 1). If this area decreases, the volume decreases, so the mass of contaminant being input should also decrease proportionally.

It can be shown that the surface masses in this system also satisfy Eq. (3) for $Q = N - N_D + P - C + C_D$, the biomass analogue. However, the introduction of two clustering species means that the surface masses do not satisfy Eqs. (4)–(5). The coextensive clustering of c and p completely changes the dynamics of the system, by increasing the efficiency of the mixing process between them.

It can be shown that a new equilibrium exists in the long time limit of clustering, which can be given implicitly in terms of the equilibrium contaminant concentration (see Appendix C):

$$C_D(P) = N_D - P - \frac{N_D N_\infty}{N_\infty + P}. \tag{34}$$

This formula does not define a P for all values of C_D. Specifically, there is no non-zero equilibrium for:

$$C_D > (\sqrt{N_D} - \sqrt{N_\infty})^2\,, \tag{35}$$

which means that the plankton population undergoes total extinction at a much lower value of C_D. Also, the onset of extinction is now an abrupt discontinuous change, in contrast to the no clustering case.

This equilibrium represents a situation in which the majority of mass of floating tracer is attracted into the densest clusters, which occurs exponentially (Koshel et al., 2019). This leads to the global balance of the biogeochemical system being dominated by the reactions within clusters. Inside the clusters, concentration of both plankton and microplastics are elevated, this leads to an increase in the global rate of interaction increases and a much greater negative impact of the contaminant.

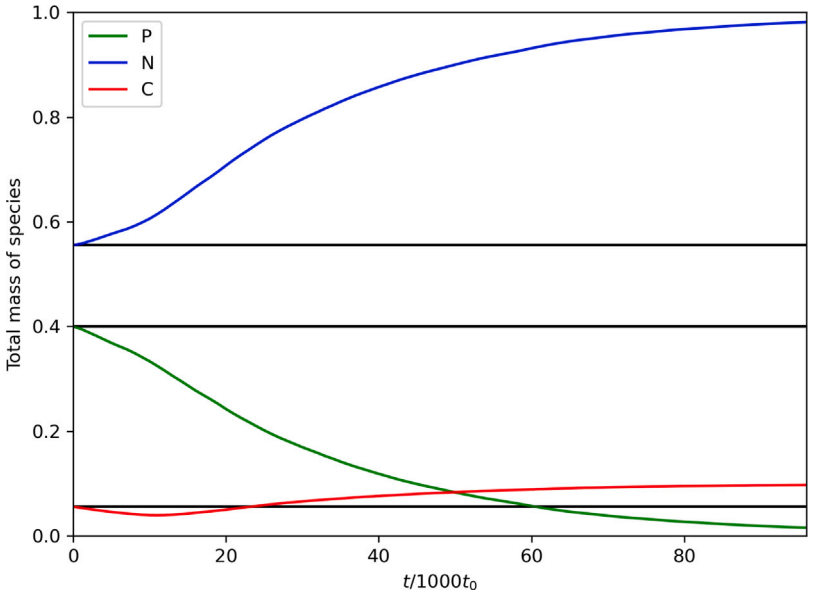

Fig. 2. An example of surface mass integrals for $C_D = 0.1, \gamma = 0.1$, we can see how the original equilibrium is made unstable by the clustering process. In this case, the global integrals converge on the only remaining stable equilibrium, $N = N_D, C = C_D, P = 0$. The black lines show the equilibrium of the ODE model (Eqs. (6)–(8)), at which the clustering simulation was initialised. The time axis is scaled by $1000t_0$ where t_0 is the memory timescale of the kinematic flow (see Appendix C).

The quantity λC_D represents the rate of introduction of contaminant into the system, but through re-scaling of dimensions, is also related to the strength of interaction between P and C. For more realistic weak interactions, we can see that the impact of clustering is still significant. A Taylor expansion at $C_D = 0$ gives:

$$P \approx P_\infty + \left.\frac{dC_P}{dP}\right|_{P_\infty} (P - P_\infty), \tag{36}$$

where $P_\infty = N_D - N_\infty$ is the equilibrium plankton mass in the NP equations (1)–(2). Using Eq. (34):

$$P \approx N_D - N_\infty - \frac{N_D}{N_D - N_\infty} C_D . \tag{37}$$

In comparison with Eq. (7), we see that the impact of the contaminant is amplified by:

$$\frac{N_D}{N_D - N_\infty} > 1 \tag{38}$$

For the choice of parameters used in our clustering simulations, this ratio is equal to two, implying that increasing the rate of contaminant introduction in our simulations leads to a reduction in the plankton population that is twice as large as in the no-clustering case (in the small C_D limit). The impact of clustering is even more significant for larger values of C_D.

Notably, the clustering equilibrium state is independent of any specifics of the velocity field. It only requires the presence of a non-zero potential component to the surface flow. The only factor dependent on the strength of clustering is the speed of convergence towards the equilibrium.

3. Clustering simulations

Our numerical experiments contain two components: a velocity model and a particle model. For the velocity model, we generate stochastic Gaussian random fields to model isotropic, homogeneous turbulence. The form of these is based on those used in Koshel et al. (2019) and identical to those in Meacham and Berloff (2023). Velocity fields are decomposed into potential and solenoidal components:

$$\mathbf{u} = \gamma \mathbf{u}_p + (1 - \gamma)\mathbf{u}_s , \tag{39}$$

$$\mathbf{u}_p = (\partial_x \phi, \partial_y \phi) \tag{40}$$

$$\mathbf{u}_s = (-\partial_y \psi, \partial_x \psi) \tag{41}$$

where $\gamma \in [0, 1]$ and ϕ, ψ are the potential and streamfunction respectively. The γ parameter allows us to exactly control the strength of our convergences, which are the force driving cluster formation. We typically choose values in the range $\gamma \approx 0.01 - 0.1$. The value of γ is analogous to the Rossby number, since this is the ratio of the magnitudes of diverging ageostrophic and non-divergent geostrophic currents. The chosen values are typical of the real ocean. Further details of velocity field construction are contained in Appendix D.

For the tracer model, we choose to solve all equations in a Lagrangian sense, by tracking a large number of particles transported by the modelled surface current. In theory, Eulerian and Lagrangian descriptions should be equivalent. In practice, discretising the equations on a finite grid necessitates introduction of unphysical diffusivities in the Eulerian case. These act to regularise solutions that would otherwise be numerically unstable by moving tracer concentration down-gradient. It has been shown that these diffusions have an unduly large impact on the clustering process (Meacham and Berloff, 2023). By adopting a Lagrangian methodology, we forgo any diffusion and focus purely on the advective mixing processes. Lagrangian particles also naturally settle in areas of intense clustering, meaning our data will resolve these regions well even for a small number of particles.

To calculate the total mass of various tracers using only discrete Lagrangian data, we first apply a change of variables to integrals (19) and (20). We integrate over initial conditions of the Lagrangian paths instead of the spatial coordinates, and then use Gaussian quadrature to estimate the integrals (See Appendix A for details). Calculating integrals in this way has high accuracy, allowing fewer particles to achieve better simulation of the global masses of tracer. Using this method requires us to initialise our particles at the two-dimensional Gaussian quadrature points. We used 10^4 Lagrangian particles for calculating these masses (100 quadrature points in each coordinate direction).

Simulations are doubly periodic such that particles that leave the domain re-enter at the opposite boundary. The velocity field is similarly doubly periodic by construction. Each model run is initialised at the equilibrium for the no-clustering case (Eqs. (6)–(8)) and is run until a new equilibrium is reached. Fig. 2 shows the three global masses for a simulation with $c_D = 0.1$, with a clear relaxation to a different steady state.

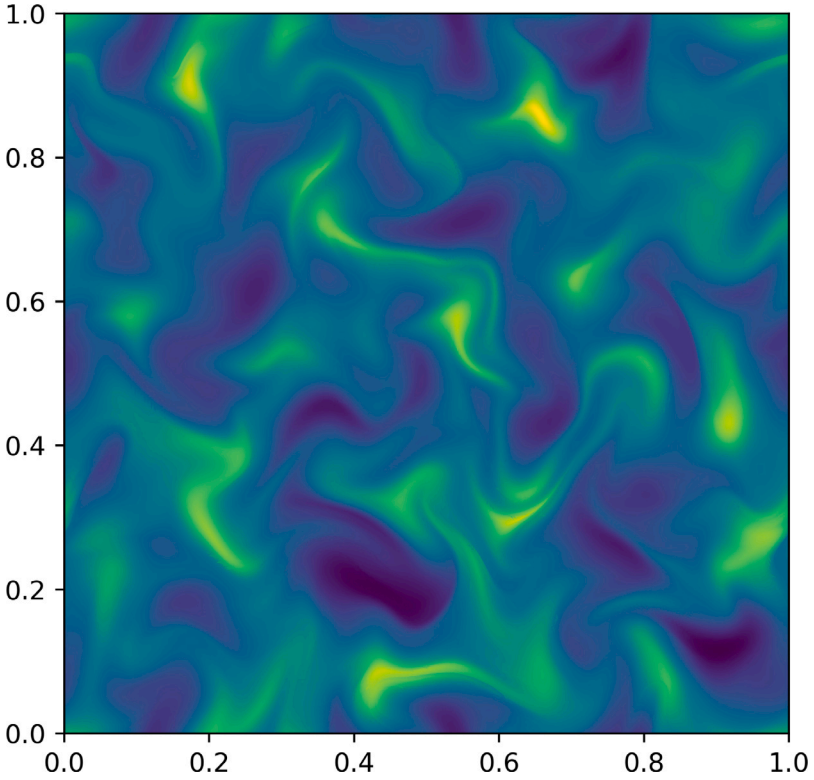

Fig. 3. An example of the contaminant concentration from a clustering simulation of an initially regular grid of 500 × 500 particles. The formation of dense clusters and sparse voids is evident here.

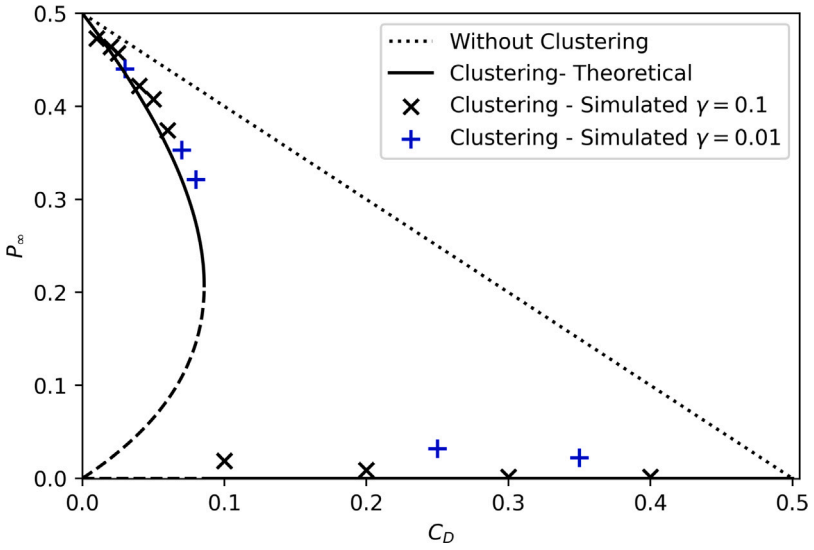

Fig. 4. Equilibrium plankton mass for several clustering simulations as a function of the equilibrium contaminant concentration C_D (each model is denoted by a cross). The solid black line is the analytic form of the equilibrium, the dotted line shows the theoretical equilibrium mass for the ODE model (without clustering).

For the NPC model, we use $\mu = 0.08, \lambda = 0.04$ and $n_D = 1.0$, so that $N_\infty = 0.5$. We run simulations for many values of c_D, in an attempt to reproduce the theoretical equilibrium (34).

To investigate the spatial distribution of the tracer concentrations, we also initialise 500 × 500 particles in a regular grid. An example of the contaminant concentration c is contained in Fig. 3. This shows the qualitative features of the clusters formed in these kinematic velocity fields. The effect of filamentation by the solenoidal part of the velocity can clearly be seen, as well as the extreme inhomogeneity of the concentration distribution.

4. Results

Our results confirm the structure of the equilibrium plankton mass agrees with Eq. (34). We choose two values of γ, the parameter controlling the strength of the divergence, to demonstrate the independence of this equilibrium on the particular structure of the velocity field. Both of these points are illustrated in Fig. 4.

The effect on the dynamics is evident for all contaminant concentrations c_D, but the most severe impact is the reduction in the rate of contaminant introduction required to reduce the plankton mass to zero.

With the parameters used here, the rate of contaminant introduction required is approximately $\frac{1}{5}$ lower in the presence of the clustering process, but can be even lower depending on the values of N_D and $N_\infty = \frac{\lambda}{\mu}$. Additionally, the dependence of the plankton mass loss on the rate of addition of contaminant was shown to be larger in the presence of clustering, even for infinitesimally small c_D (see Fig. 4 and Appendix B). By dimensional scaling, the strength of contaminant introduction can also be understood as the strength of interaction between plankton and contaminant. In this way, we can see that the ecological risk is significantly enhanced even for weak interaction, due to the larger gradient $\left|\frac{dP}{dC_D}\right|$ near $C_D = 0$. This gradient is doubled for our choice of parameters.

Although the end state of our system is independent of our velocity field, the time taken to reach this end state will vary greatly based on the strength of the potential component of the flow. Our derivation in Appendix C shows that the relaxation to this equilibrium depends on a timescale proportional to the inverse of the variance of the divergence. It was shown in Klyatskin (2003) and Koshel et al. (2019) that for our kinematic fields, this relevant timescale is $\tau = l^2/\gamma^2 t_0 \sigma_{\mathbf{u}}^2$. Here, t_0 is the decorrelation timescale, γ is the Rossby number and $\sigma_{\mathbf{u}}$ is the velocity variance. If the source of clustering is the submesoscale ocean currents, we can take reasonable values to show that this timescale could range from $1-2$ weeks to $\sim$100 days.

5. Summary and discussion

Aggregations of marine plastic pollution have been observed in multiple 'accumulation zones'. Additionally, filaments evident in the distribution of plankton in the ocean suggest that the spatial form of the ocean currents imprint heavily on both distributions. One mechanism for this is clustering due to non-zero buoyancy forces. Floating plastic contaminants are known to be a hazard to marine life, especially since they accumulate hydrophobic toxins including POPs (Persistent Organic Pollutants) (Andrady, 2011). However, it is an open question if the formation of these dense clusters of marine contaminants represents an enhanced risk to the oceanic food web. To answer this question requires modelling of the mixing processes in the upper ocean.

We find that the inclusion of the leading order inertial effects of particle buoyancy leads to a host of new physical considerations when constructing interacting tracer models. For example, the form of interaction terms depending on the differing tracer velocities is altered. Using insights from our idealised model, the road to more complex and realistic models is clear. The severe effect of clustering of ocean contaminants, even in our simple model, provides motivation for further study of this phenomenon.

When there is more than one buoyant species in the biogeochemical system, both are arranged into clusters and voids by the convergent surface currents. Due to the very high density inside the clusters, the reaction rates are increased there. Given enough time has passed, this allows for a novel equilibrium state in which the global state of the system is dominated by reactions within the clusters as the plankton and contaminant masses are continually drawn into the densest regions. This is an example of the potential for significantly enhanced mixing as a result of buoyancy forces and surface clustering, and it depends very little on the specifics of the model.

It is possible that this new equilibrium could be degraded by diffusive processes, or in more realistic ocean models where clustering may have a very different character. However, the independence of the equilibrium in our model on the particulars of the velocity field implies that such effects could be surprisingly robust. Verifying that our results are still valid in a dynamically constrained flow is an important incremental next step in this research direction. In the long term, parameterising the effect of buoyant clustering on oceanic mixing and biogeochemical reactions for inclusion in climate type models will help constrain the global distribution of plastic pollutants, and the magnitude of the risk they entail to marine life. This can only be achieved once the small scale dynamics of clustering are understood. Furthermore, the coupling of biological reactions to the details of the ocean flow leads to a scenario where accurate modelling can only be achieved through an interdisciplinary approach. Advancing away from idealised models to a realistic description will require insights from biological, oceanographic and transport theories.

CRediT authorship contribution statement

Jamie Meacham: Conceptualization, Data curation, Formal analysis, Investigation, Methodology, Project administration, Resources, Software, Supervision, Validation, Visualization, Writing – original draft, Writing – review & editing. **Pavel Berloff:** Conceptualization, Data curation, Formal analysis, Investigation, Methodology, Resources, Software, Supervision, Validation, Visualization, Writing – original draft, Writing – review & editing.

Declaration of competing interest

The authors declare that they have no known competing financial interests or personal relationships that could have appeared to influence the work reported in this paper.

Data availability

Data will be made available on request.

Acknowledgements

Pavel Berloff was supported by the Leverhulme Trust, United Kingdom Grant RPG-2019-024, by the Natural Environment Reasearch Council (NERC) Grant NE/T002220/1 and by the Moscow Centre for Fundamental and Applied Mathematics, Russia (supported by the Agreement 075-15-2019-1624 with the Ministry of Education and Science of the Russian Federation, Russia). We would like to thank the reviewers for their detailed analysis of our manuscript, which benefited greatly from their input.

Appendix A. Clustering area and surface masses

A material area at the ocean surface is an area that moves with the horizontal surface flow. i.e. we can find the area at a later time by advecting all points inside the area and on the boundary. In the limit of vanishing area, the change in scale of an area over time becomes the flow map Jacobian of the transformation $\mathbf{x}_0 \to \mathbf{x}(t;\mathbf{x}_0)$. i.e.

$$\frac{A(t)}{A(0)} \equiv |\mathbf{J}(t)|\,, \tag{A.1}$$

where the flow map Jacobian is defined as:

$$|\mathbf{J}| = \det\begin{bmatrix} \frac{\partial x}{\partial x_0} & \frac{\partial y}{\partial x_0} \\ \frac{\partial x}{\partial y_0} & \frac{\partial y}{\partial y_0} \end{bmatrix}. \tag{A.2}$$

Differentiating this determinant with respect to time along Lagrangian paths and using the fact that $\frac{d\mathbf{x}}{dt} = \mathbf{u}$ leads to:

$$\frac{d}{dt}|\mathbf{J}| = |\mathbf{J}|\nabla\cdot\mathbf{u}\,, \tag{A.3}$$

which is the derivation of Eq. (11). By the conservation of volume of passive tracer, we also have that $|\mathbf{J}| = 1/h$.

For a passive tracer with density ρ that is conserved along Lagrangian paths, it can be shown that:

$$\int_D d^2\mathbf{x}\,\rho(\mathbf{x},t)\,, \tag{A.4}$$

is not conserved. This is because the above integral does not represent the total mass of passive tracer at the surface, due to the fact that the

vertical velocity below the surface is non-zero. Introducing an arbitrary kernel to this integral:

$$I = \int_D d^2\mathbf{x}\, K(\mathbf{x},t)\rho(\mathbf{x},t) \tag{A.5}$$

We can use a change of variables $\mathbf{x} \to \mathbf{x}_0$, which introduces a factor of the Jacobian $|\mathbf{J}|$, since $d^2\mathbf{x} = |\mathbf{J}|d^2\mathbf{x}_0$.

$$I = \int_D d^2\mathbf{x}_0\, |\mathbf{J}| K(\mathbf{x}(t;\mathbf{x}_0),t)\rho(\mathbf{x}(t;\mathbf{x}_0),t) \tag{A.6}$$

taking a time derivative here and applying Eqs. (16) and (A.3), we find that the appropriate kernel to conserve this integral is $K = 1/|\mathbf{J}| = h$. This is an intuitive result, since $h\, d^2\mathbf{x}$ is proportional to the volume of an infinitesimal material element of passive tracer just below the surface. This quantity is therefore the surface mass of passive tracer.

A similar change of variables is used to calculate surface masses from Lagrangian data.

For buoyant tracers:

$$M_C(t) = \int_D C(\mathbf{x}(t;\mathbf{x}_0),t)|\mathbf{J}|(t,\mathbf{x}_0)d^2\mathbf{x}_0 \tag{A.7}$$

If we initialise a square number $N = n^2$ particles at the 2D Gaussian quadrature points $\mathbf{a}_{ij}$, we can approximate the surface mass using the Gaussian quadrature formula:

$$M_C(t) \approx \sum_{i=1}^{n}\sum_{j=1}^{n} w_{ij} C(\mathbf{x}(t;\mathbf{a}_{ij}),t)|\mathbf{J}|(t,\mathbf{x}_{ij})\,, \tag{A.8}$$

where w_{ij} are the Gaussian quadrature weights. Estimating integrals in this way has desirable convergence properties, allowing use of fewer particles in the simulation to achieve greater accuracy in the global masses of tracer. For a passive tracer with density ρ, similar considerations lead to:

$$M_\rho(t) \approx \sum_{i=1}^{n}\sum_{j=1}^{n} w_{ij}\rho(\mathbf{x}(t;\mathbf{a}_{ij}),t)\,. \tag{A.9}$$

Appendix B. NP tracer model solution

It can be shown that global masses for buoyant plankton and passive nutrients in the system of Eqs. (22)–(25) exactly satisfy Eqs. (1)–(2). If we take the following ansatz for the solution:

$$p = P(t)h(\mathbf{x},t)\,, \tag{B.1}$$

$$n = N(t)\,. \tag{B.2}$$

By integrating over the domain, it can be shown that $P(t)$ and $N(t)$ are the surface masses of plankton (26) and nutrients (27) respectively. If we substitute this ansatz into the Eqs. (22)–(23), we recover the Eqs. (1)–(2). Since the solution is unique, it shows that clustering leads to no new dynamics in this model, and this has been verified through numerical experiments. This could be seen as an expected result, since there is no coextensive clustering between species. The plankton population forms clusters, but the passivity of the nutrients means that they stay uniformly distributed.

Appendix C. Clustering equilibrium

We can recast the NPC tracer equations in terms of the mass of each species inside a surface element $\rho = p|\mathbf{J}|$, $\Gamma = c|\mathbf{J}|$ (recalling that $|\mathbf{J}|$ is proportional to the surface area of a material element). This leads to:

$$\frac{dn}{dt} = -\mu n\rho - \lambda(n - n_D)\,, \tag{C.1}$$

$$\frac{d\rho}{dt} = \mu n\rho - \frac{\mu}{|\mathbf{J}|}\rho\Gamma - \lambda\rho\,, \tag{C.2}$$

$$\frac{d\Gamma}{dt} = -\frac{\mu}{|\mathbf{J}|}\rho\Gamma - \lambda(\Gamma - c_D)\,. \tag{C.3}$$

Motivated by the 'conserved' quantity of our equations, we can show that in the limit $t \to \infty$:

$$n - n_D + \rho - \Gamma + c_D = 0 \tag{C.4}$$

which substitutes directly back into Eq. (C.2), to give:

$$\frac{d\rho}{dt} = \mu n\rho - \lambda\rho - \frac{\mu}{|\mathbf{J}|}\rho[n - n_D + \rho + c_D]\,. \tag{C.5}$$

If our velocity field divergence were delta-correlated in both time and space, with zero mean, it can be shown (through solving the appropriate Fokker–Planck equation) that $\ln|\mathbf{J}(t)|$ is normally distributed with p.d.f.:

$$f(x) = \frac{1}{\sqrt{4\pi D(t-t_0)}}\exp\left(-\frac{x^2}{4D(t-t_0)}\right), \tag{C.6}$$

where $D(>0)$ is proportional to the variance of the divergence. This further implies that:

$$\left\langle \frac{1}{|\mathbf{J}(t)|} \right\rangle = e^{D(t-t_0)} \tag{C.7}$$

Hence, looking at Eq. (C.5), it becomes clear that $\frac{\mu}{|\mathbf{J}|}\rho[n-n_D+\rho+c_D]$ is the dominant term on average. Hence, in order to achieve non-trivial equilibrium at late times it must be zero. This can be used to eliminate ρ in the nutrients equation. Integrating over initial conditions with $dN/dt = 0$ and using $P + N = C_D + N_D$, we can express the resulting plankton mass implicitly in terms of C_D, N_D, N_∞:

$$C_D = N_D - P - \frac{N_\infty N_D}{N_\infty + P} \tag{C.8}$$

Furthermore, by finding the point (P, C_D) at which $\frac{dC_D}{dP} = 0$, we can find the maximum C_D where a non-zero steady plankton population can exist:

$$P = \sqrt{N_\infty}(\sqrt{N_D} - \sqrt{N_\infty})\,, \tag{C.9}$$

$$C_D = (\sqrt{N_D} - \sqrt{N_\infty})^2\,. \tag{C.10}$$

At small C_D values, we can take a Taylor expansion about the $C_D = 0$ solution, $P = N_D - N_\infty$, to see the impact of clustering in this limit. To leading order, Eq. (C.8) becomes:

$$P \approx N_D - N_\infty - \frac{N_D}{N_D - N_\infty}C_D\,. \tag{C.11}$$

This contrasts with Eq. (7), since there is a steeper gradient with respect to the contaminant C_D. Hence, pollutants are significantly more potent in the presence of clustering, even in this limit.

Appendix D. Velocity model

The velocity fields utilised in this study are identical to the time-correlated kinematic fields used in Meacham and Berloff (2023). The velocity is decomposed into potential (divergent) and solenoidal (non-divergent) components. The strength of the potential component, which causes clustering, is controlled through a parameter γ.

$$\mathbf{u} = \gamma\mathbf{u}_p + (1-\gamma)\mathbf{u}_s\,. \tag{D.1}$$

The components of the velocity field $(\mathbf{u}_p, \mathbf{u}_s)$ are decomposed in terms of scalar spectral coefficients a_p, b_p, a_s, b_s. For example, the potential component is expressed as:

$$\mathbf{u}_p = \int d^2\mathbf{k}\left(a_s(\mathbf{k},t) + ib_s(\mathbf{k},t)\right)\frac{\mathbf{k}}{k}\exp(i\mathbf{k}\cdot\mathbf{x})\,. \tag{D.2}$$

Each coefficient is independent of every other, and satisfies a Langevin equation at every wavenumber:

$$\frac{d}{dt}a_p(\mathbf{k},t) = -\lambda a_p(\mathbf{k},t) + \eta(\mathbf{k},t)\,. \tag{D.3}$$

$$\left\langle \eta(\mathbf{k}', t')\eta(\mathbf{k}, t)\right\rangle = 2\lambda\sigma_{\mathbf{u}}^2 E(k)\delta(\mathbf{k}' - \mathbf{k})\delta(t - t'), \tag{D.4}$$

this leads to exponentially decaying flow memory, with decorrelation timescale $t_0 = \frac{1}{\lambda}$. The function $E(k)$ imposes the power spectrum for the kinetic energy of the flow. To mimic homogeneous, isotropic turbulence, we follow Koshel and use the spectrum:

$$E(k) = \frac{1}{2\pi}\frac{k^2 l^4}{4}\exp\left(-\frac{k^2 l^2}{2}\right). \tag{D.5}$$

This simple form of this spectrum has qualitative similarity to the narrow band structure of traditional Kolmogorov turbulence. Its analytic simplicity also allows for the explicit calculation of statistical quantities.

References

Andrady, A.L., 2011. Microplastics in the marine environment. Mar. Pollut. Bull. 62 (8), 1596–1605. http://dx.doi.org/10.1016/j.marpolbul.2011.05.030, URL: https://www.sciencedirect.com/science/article/pii/S0025326X11003055.

Della Rossa, F., Fasani, S., Rinaldi, S., 2013. Conditions for patchiness in plankton models. Theor. Popul. Biol. 83, 95–100. http://dx.doi.org/10.1016/j.tpb.2012.10.003, URL: https://www.sciencedirect.com/science/article/pii/S0040580912000986.

Flynn, K.J., McGillicuddy, D.J., 2018. Modeling marine harmful algal blooms: Current status and future prospects. In: Harmful Algal Blooms. John Wiley & Sons, Ltd, pp. 115–134. http://dx.doi.org/10.1002/9781118994672.ch3, URL: https://onlinelibrary.wiley.com/doi/abs/10.1002/9781118994672.ch3. arXiv:https://onlinelibrary.wiley.com/doi/pdf/10.1002/9781118994672.ch3.

Franks, P., 2002. NPZ models of plankton dynamics: Their construction, coupling to physics, and application. J. Oceanogr. 58, 379–387. http://dx.doi.org/10.1023/A:1015874028196.

Gower, J., Hu, C., Borstad, G., King, S., 2006. Ocean color satellites show extensive lines of floating sargassum in the gulf of Mexico. IEEE Trans. Geosci. Remote Sens. 44 (12), 3619–3625. http://dx.doi.org/10.1109/TGRS.2006.882258.

Klyatskin, V., 2003. Clustering and diffusion of particles and passive tracer density in random hydrodynamic flows. Phys.-Usp. 46, 667–688.

Koshel, K.V., Stepanov, D.V., Ryzhov, E.A., Berloff, P., Klyatskin, V.I., 2019. Clustering of floating tracers in weakly divergent velocity fields. Phys. Rev. E 100, 063108. http://dx.doi.org/10.1103/PhysRevE.100.063108, URL: https://link.aps.org/doi/10.1103/PhysRevE.100.063108.

Martin, A., 2003. Phytoplankton patchiness: the role of lateral stirring and mixing. Prog. Oceanogr. 57 (2), 125–174. http://dx.doi.org/10.1016/S0079-6611(03)00085-5, URL: https://www.sciencedirect.com/science/article/pii/S0079661103000855.

Matthews, L., Brindley, J., 1997. Patchiness in plankton populations. Dyn. Stab. Syst. 12 (1), 39–59. http://dx.doi.org/10.1080/02681119708806235, arXiv:https://doi.org/10.1080/02681119708806235.

Meacham, J., Berloff, P., 2023. On clustering of floating tracers in random velocity fields. J. Adv. Modelling Earth Syst. 15 (5), e2022MS003484. http://dx.doi.org/10.1029/2022MS003484, arXiv:https://agupubs.onlinelibrary.wiley.com/doi/pdf/10.1029/2022MS003484. URL: https://agupubs.onlinelibrary.wiley.com/doi/abs/10.1029/2022MS003484. e2022MS003484 2022MS003484.

Onink, V., Wichmann, D., Delandmeter, P., van Sebille, E., 2019. The role of ekman currents, geostrophy, and Stokes drift in the accumulation of floating microplastic. J. Geophys. Res.: Oceans 124 (3), 1474–1490. http://dx.doi.org/10.1029/2018JC014547, URL: https://agupubs.onlinelibrary.wiley.com/doi/abs/10.1029/2018JC014547. arXiv:https://agupubs.onlinelibrary.wiley.com/doi/pdf/10.1029/2018JC014547.

Prend, C.J., Flierl, G.R., Smith, K.M., Kaminski, A.K., 2021. Parameterizing eddy transport of biogeochemical tracers. Geophys. Res. Lett. 48 (21), e2021GL094405. http://dx.doi.org/10.1029/2021GL094405, arXiv:https://agupubs.onlinelibrary.wiley.com/doi/pdf/10.1029/2021GL094405. URL: https://agupubs.onlinelibrary.wiley.com/doi/abs/10.1029/2021GL094405. e2021GL094405 2021GL094405.

Reartes, C., Mininni, P.D., 2023. Dynamical regimes and clustering of small neutrally buoyant inertial particles in stably stratified turbulence. Phys. Rev. Fluids 8, 054501. http://dx.doi.org/10.1103/PhysRevFluids.8.054501, URL: https://link.aps.org/doi/10.1103/PhysRevFluids.8.054501.

Stepanov, D.V., Ryzhov, E.A., Berloff, P., Koshel, K.V., 2020a. Floating tracer clustering in divergent random flows modulated by an unsteady mesoscale ocean field. Geophys. Astrophys. Fluid Dyn. 114 (4–5), 690–714. http://dx.doi.org/10.1080/03091929.2020.1786551, arXiv:https://doi.org/10.1080/03091929.2020.1786551.

Stepanov, D.V., Ryzhov, E.A., Zagumennov, A.A., Berloff, P., Koshel, K.V., 2020b. Clustering of floating tracer due to mesoscale vortex and submesoscale fields. Geophys. Res. Lett. 47 (3), e2019GL086504.

van Sebille, E., Wilcox, C., Lebreton, L., Maximenko, N., Hardesty, B.D., van Franeker, J.A., Eriksen, M., Siegel, D., Galgani, F., Law, K.L., 2015. A global inventory of small floating plastic debris. Environ. Res. Lett. 10 (12), 124006. http://dx.doi.org/10.1088/1748-9326/10/12/124006.